J. Fluid Mech. (1995), *vol.* 302, *pp.* 287–305

The bifurcation of steady gravity water waves in (R, S) parameter space

By S. H. DOOLE[1] AND J. NORBURY[2]

[1]Department of Engineering Mathematics, Bristol University, Queen's Building, University Walk, Bristol BS8 1TR, UK

[2]Mathematical Institute, Oxford University, 24–29 St. Giles', Oxford OX1 3LB, UK

(Received 29 September 1994 and in revised form 29 June 1995)

The bifurcation of steady periodic waves from irrotational inviscid streamflows is considered. Normalizing the flux Q to unity leaves two other natural quantities R (pressure head) and S (flowforce) to parameterize the wavetrain. In a well-known paper, Benjamin & Lighthill (1954) presented calculations within a cnoidal-wave theory which suggested that the corresponding values of R and S lie inside the cusped locus traced by the sub- and supercritical streamflows. This rule has been applied since to many other flow scenarios. In this paper, regular expansions for the streamfunction and profile are constructed for a wave forming on a subcritical stream and thence values for R and S are calculated. These describe, locally, how wave branches in (R, S) parameter space point inside the streamflow cusp. Accurate numerics using a boundary-integral solver show how these constant-period branches extend globally and map out parameter space. The main result is to show that the large-amplitude branches for all steady Stokes' waves lie surprisingly close to the subcritical stream branch. This has important consequences for the feasibility of undular bores (as opposed to hydraulic jumps) in obstructed flow. Moreover, the transition from the 'long-wave region' towards the 'deep-water limit' is characterized by an extreme geometry, both of the wave branches and how they sit inside each other. It is also shown that a single (Q, R, S) triple may represent more than one wave since the global branches can overlap in (R, S) parameter space. This non-uniqueness is not that associated with the known premature maxima of wave properties as functions of wave amplitude near waves of greatest height.

1. Introduction

A classical free-boundary problem arises from consideration of a two-dimensional steady inviscid incompressible flow over a horizontal plane. The upper (free) surface is taken to be at constant atmospheric pressure. The analysis of such a model has included investigation of the existence and nature of periodic solutions, and would hope to yield criteria describing the relative stability of flows (uniform stream or wave) in a sensible way. From an engineering perspective on channel flow, what is important is usually the maintenance of a smooth profile, for then walls can be built easily to prevent flooding, or the flux through the channel may be controlled. Thus we are led to finding an appropriate parameter space and locating where wave solutions lie.

We state the equations for gravity waves in terms of the streamfunction ψ. The field equation is thus

$$\Delta\psi = 0, \tag{1.1}$$

where the independent variables are horizontal distance x and upwards vertical distance y. The equations can be considered to arise from the three physical principles of conservation of mass, energy and momentum (flux). The mass or volume flux (denoted Q) will be set to unity, along with gravity, via a consistent non-dimensionalization (§2). The flux appears explicitly in the kinetic condition at the upper free surface $y = \eta(x)$, $x \in \mathbf{R}$,

$$\psi(x, \eta(x)) = Q \equiv 1. \tag{1.2}$$

Equation (1.2) represents ψ being normalized by making it zero on the channel bottom so that $\psi(x, 0) = 0$, $x \in \mathbf{R}$. The extra condition on the wave surface (to compensate for its unknown location) is derived by integrating the Euler equations and is given by Bernoulli's equation,

$$\tfrac{1}{2} |\nabla\psi|^2|_{y=\eta} + g\eta(x) = R. \tag{1.3}$$

The constant R, known as the pressure head, represents energy. There is a normalization of pressure p hidden in R since we take the external pressure acting on the fluid at the upper surface to be zero.

Momentum (flux) in the x-direction is represented by the flowforce S. That is, S is the horizontal momentum flux of the fluid, modified with pressure and scaled by the density ρ, defined by (the horizontal velocity is $u = \psi_y$)

$$S := \int_0^\eta \left\{ \frac{p}{\rho} + \psi_y^2 \right\} \mathrm{d}y. \tag{1.4}$$

The three quantities Q, R and S have clear physical links. However, whilst Q and R have always been considered in progressive wave theory, S fell into disuse (until recently) after its introduction by Kelvin (1886). The definition of S is deceptive as it is easily shown to be constant in x by use of Bernoulli's theorem in the interior and integration by parts.

The flowforce S and its variants have been much studied recently by those who consider the Euler equations as an infinite-dimensional Hamiltonian system. The relevant literature is now large; see, for example Benjamin & Olver (1982), Olver (1982), Radder (1992), which consider a temporal Hamiltonian whilst Bridges (1992) describes a spatial Hamiltonian structure. Bridges (1992) shows that the spatial Hamiltonian can be completely described in terms of the energy and momentum fluxes. Also worthy of note are Benjamin (1984) and Mielke (1991).

However, the attractions of an 'energy' *vs.* 'momentum (flux)' representation are not just theoretical. From a practical viewpoint, it had been revived by Benjamin & Lighthill (1954, denoted hereafter by BL). The engineering paradigm transitions of the bore and sluice are easily identified in (R, S) parameter space and are shown in figure 1. Despite the dual appeal of this parameter space, to our knowledge, the precise location in the (R, S)-diagram of (large- and small-amplitude) waves has not appeared previously. This is the task we address in the paper. BL made various conjectures on this matter based on cnoidal-wave calculations, some of which were established by Keady & Norbury (1975, 1978). In figure 2, we show the published bounds. The hatched area shows the previously conjectured region in (R, S) parameter space where all steady waves may lie. The streamflow boundaries were conjectured

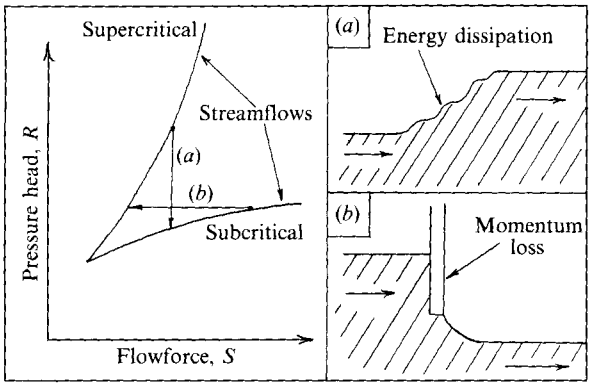

FIGURE 1. Flow transitions in the (R, S)-diagram: (a) the bore, (b) the sluice (or hydroplane).

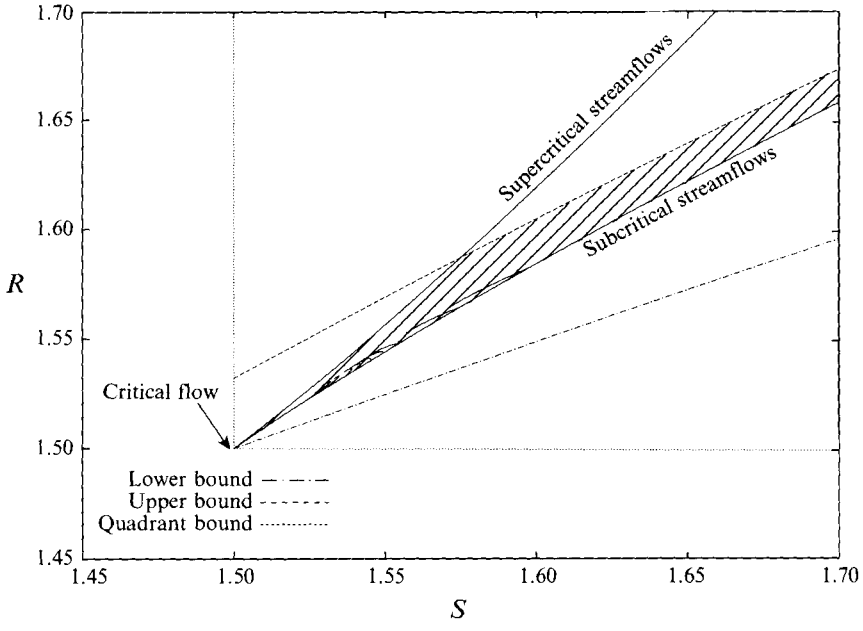

FIGURE 2. Analytical bounds of Keady & Norbury (1975), waves and streamflows in the (R, S)-diagram. Hatched region shows the conjectured domain for all possible wave flows.

by BL, and the large-amplitude wave bounds are due to Keady & Norbury (1975). Very recently, Benjamin (1995) has given an analytical argument which establishes the lower streamflow bound for monotone Stokes' waves. Our orientation of the diagram is not that of BL, but is preferred to ease discussion of incipient-branch direction (§3) and in order that it more closely resembles a normal bifurcation diagram. Note that the bounds are, in fact, very weak: typical wave branches lie in an extremely narrow strip close to the subcritical branch.

The wave branches are shown in greater detail in figure 3. (h_p is a mean wave depth, arising in the numerical method (§4), which is used in §5 to parameterize the investigation of bifurcation from the subcritical branch.) The envelope of these wave branches provides a 'third barrier' (upper bound) on the possible 'wave drag' (momentum flux loss) at constant energy (R) if an obstructed flow is to have down-

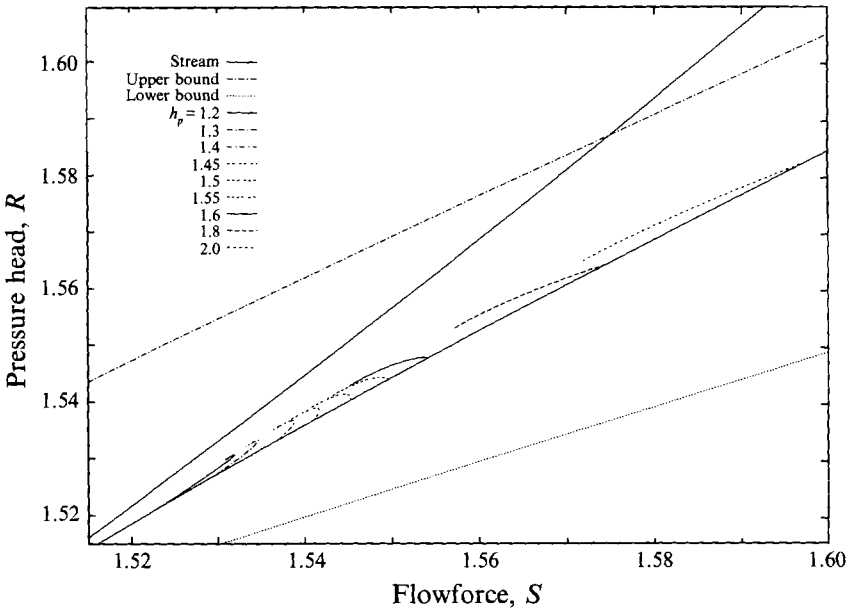

FIGURE 3. The irrotational (R, S)-diagram and analytical bounds with wave branches for $h_p = 1.1$, 1.2, 1.3, 1.4, 1.45, 1.5, 1.55, 1.6, 1.8 and 2.0.

stream waves. What is clear is that, for most depths, if the momentum loss is greater than about a third of $S_{sub} - S_{super}$ then an undular transition is not possible. Only a jump to the supercritical stream can be achieved. In fact, for the flowforce greater than say, $S \geqslant 1.59$ (6% above critical), momentum loss in transitions from subcritical streams to wave flows cannot exceed (around) 20% of the loss involved in jumping to a supercritical stream.

In § 3, second-order regular perturbation series are constructed to locate the waves close to their onset in the (R, S)-diagram. It is shown that, as expected, small-amplitude waves lie inside the cusped locus of streamflows. Such convictions have a long history. Ursell (1953) showed that for linearized flow theory to be applicable not only did ak and a/d have to be small, but a/k^2d^3 as well (where a, k and d are suitable measures of amplitude, wavenumber and depth). By analysis of experimental data, BL noted that this last parameter combination was $O(1)$ in bore transitions, indicating a balance of dispersive and steepening effects. Hence they constructed a cnoidal-wave theory whose novel feature was that all the coefficients in the governing amplitude equation were combinations of Q, R and S. On the basis of calculations made for these cnoidal waves and physical considerations, it was conjectured that (for irrotational flows) all wavetrains are uniquely determined by their values of Q, R, and S; and moreover, if Q is held fixed, then R and S are constrained to lie between the values corresponding to the uniform streamflows. The work presented here confirms the latter conjecture but also shows that the former is not correct, in that for certain ranges of (R, S) parameters, the loci of wave branches overlap (figures 8 and 9). Note that this is a different type of non-uniqueness to that associated with secondary bifurcation from the Stokes' wave branch near maximum amplitude.

Despite the status of results for changes in momentum flux and total head, as late as 1989 Dixon described a surprisingly 'confused state of affairs' concerning a problem (related to ours) arising in the study of the effect of stationary disturbances

on far downstream flow. De (1955) proposed a fifth-order Stokes expansion and plotted R and S values (to understandably limited accuracy) in a transformed plane, for a stream of volume flow Q. However, his choice of loci and parameters has been criticised (Fenton 1985; Dixon 1989) and, in fact, he assumes the BL conjecture in plotting those loci. In addition, since Schwartz (1974) it has been known that De's approach based upon an expansion in the first Fourier coefficient is flawed. Moreover, Chappelear (1961) claimed, and Fenton (1985) identified, errors in De's series expansions. Both Cokelet (1977) and Williams (1981) tabulate some R and S values, but Q is not fixed, and more importantly, the emphasis is on parameter values and profiles near the extreme Stokes' 120° corner wave. The precise location of the complete wave branches in the (R, S)-diagram is not established in any of these papers, nor are the surprising results that we show in figure 2, for example, remarked upon.

In § 5, we fill this gap by presenting numerical calculations for the branches of waves in the (R, S)-plane with Q fixed, using the boundary-integral solver of Teles da Silva & Peregrine (1988), which those authors kindly supplied. We map out the changes in loci of constant-period wave branches in parameter space between the long-wave and deep-water regimes, and note how individual wave branches 'sit inside' each other. The main features are summarized by figure 3 in which the closeness of the wave branches to the subcritical stream, and the geometry of the transition in wave-branch shape from the 'long-wave' limit to the 'deep-water' region is clear.

2. The governing equations

The equations for plane gravity waves are derived from Euler's equations for steady incompressible fluid flow. The Galilean invariance of the underlying equations means that the problem of a periodic wavetrain propagating without change of form can be viewed as steady motion by the addition of a horizontal velocity to the reference frame. Moreover, by considering coordinates in which one axis (say, the x-axis) is parallel to the direction of propagation, the problem becomes two-dimensional. Hence we consider Cartesian axes (x, y, z) with y as the vertical axis in the plane to which the problem has been reduced. We state the problem in terms of the streamfunction ψ defined in the usual way. For irrotational flow, ψ satisfies Laplace's equation (1.1). The use of the streamfunction formulation leads to relatively simple expressions for the parameters of interest (compared to, say, De 1955). This advantage has already been exploited within cnoidal-wave theory by Fenton (1979).

It remains to discuss the boundary conditions. We assume that the waves are of finite depth above a horizontal bottom at $y = 0$. In addition, if the free surface has a tangent nowhere vertical, it may be written as a single-valued function $y = \eta(x)$. One deduces that ψ is equal to a constant Q, say, on the free surface, (1.2). It follows from the definition of ψ that we may take Q to be the volume flux of the channel flow. We assume $Q > 0$ (which implies that η is strictly positive), so that the apparent flow is from left to right, in the direction of x increasing. The dynamic boundary condition is derived by integrating Euler's equations using the free-surface constant-pressure assumption, and is given by (1.3) for R, the total, or pressure, head.

Let $2L$ be the wavelength of periodic waves arranged so that η is $2L$-periodic, ψ is $2L$-periodic in x and $\eta'(\pm L) = 0$. From periodicity considerations, we impose the boundary conditions

$$\psi_x(\pm L, y) = 0, \tag{2.1}$$

which ensure that the boundary value problem for ψ given η is well posed. For representation in the (R, S)-plane, we scale Q and g out of the problem (but the non-dimensional wavelength remains). Both are scaled to unity via

$$\psi = Q\hat{\psi}, \qquad x = (Q^2/g)^{1/3}\hat{x}, \tag{2.2}$$

with y scaled as for x. Dropping hats, we obtain the following problem: find $\psi(x, y)$, $\eta(x)$ and $L > 0$ such that

$$\Delta\psi = 0, \qquad x \in (-L, +L), \quad 0 < y < \eta(x), \tag{2.3}$$

$$\psi(x, 0) = 0, \qquad x \in [-L, +L], \tag{2.4}$$

$$\psi_x(\pm L, y) = 0, \qquad y \in [0, \eta(\pm L)], \tag{2.5}$$

$$\psi(x, \eta(x)) = 1, \qquad x \in [-L, +L], \tag{2.6}$$

$$\tfrac{1}{2}|\nabla\psi(x, \eta(x))|^2 + g_1\eta(x) = R = \text{const}, \quad x \in [-L, +L]. \tag{2.7}$$

We denote this as problem $[P_\eta]$. Here L is a parameter, and we consider a branch of waves of varying amplitude and of fixed wavelength $2L$. Along such a branch, R will vary and so will S, defined by (1.4) but more conveniently rewritten as

$$S = \int_0^\eta (R - y - \tfrac{1}{2}\psi_x^2 + \tfrac{1}{2}\psi_y^2)\mathrm{d}y, \tag{2.8}$$

by using Bernoulli's theorem throughout the fluid to eliminate the pressure, and our scaling. The half-period L can be thought of as providing an extra axis in parameter space, parallel to which we project all solution branches onto the (R, S)-diagram. Our strategy is to solve (2.3)–(2.7) for ψ and η (given L) and thus R. Then with such ψ and η, we find S corresponding to R. Note that at $x = \pm L$, (2.8) yields (using (2.5))

$$S = R\eta - \tfrac{1}{2}\eta^2 + \tfrac{1}{2}\int_0^\eta \psi_y^2 \mathrm{d}y. \tag{2.9}$$

In the next section, we do this analytically for small-amplitude waves. The reader who is only interested in the global branch behaviour should go immediately to § 5.

3. Perturbation theory in (R, S) parameter space

In this section, we investigate the onset of gravity waves in (R, S) parameter space, local to the streamflow from which they bifurcate. One-dimensional streamflow solutions of (2.3)–(2.6) are given by $\bar{\psi}(y) = y/h$, $\eta \equiv h$, where h satisfies

$$S_h = \frac{h^2}{2} + \frac{1}{h}, \qquad R_h = \frac{1}{2h^2} + h. \tag{3.1}$$

Both R_h and S_h have a unique minimizing depth $h_* = 1$. The smaller (shallower) solution (for R, $S > R_*$, $S_* = 3/2$ respectively) is the supercritical flow depth h_- and the larger (deeper) is the subcritical flow depth, h_+ (Keady & Norbury 1975, 1978). What we wish to determine is how the values of the pressure head R and the flowforce S for such waves compare to those R_h, S_h values for a streamflow. To do so, we calculate a weakly nonlinear solution by finding a second-order correction to the streamflow.

We use ϵ as a (non-dimensional) perturbation parameter. This is a parameterization related to amplitude along the curve in (R, S)-space that represents a wave branch. Globally, of course, such a parameterization is required because of the multi-valuedness of any functional dependence $S = S(R)$ or $R = R(S)$. The choice of this parameter ϵ related, but not equal, to amplitude (within the streamfunction

formulation) is made for convenience. The unfolding of wave properties is then much more straightforward than with a more conventional approach. Our corrections are sufficiently simple that one can see explicitly their sign and the slope of the incipient wave branch (compare De 1955, for example). We discuss at the end of this section how to eliminate ϵ to obtain $R = R(S)$ (or equivalently ϵ in terms of physical parameters).

We solve, at successive orders, (2.3)–(2.6) and then calculate from (2.7)–(2.8) the corrections to R_h and S_h, the head and flowforce, respectively, of the streamflow. The *ansatz* is

$$\left.\begin{aligned} \psi(x,y) &= \psi_o(y) + \epsilon\psi_1(x,y) + \epsilon^2\psi_2(x,y) + O(\epsilon^3), \quad & R &= R_o + \epsilon R_1 + \epsilon^2 R_2 + O(\epsilon^3), \\ \eta(x) &= h + \epsilon\eta_1(x) + \epsilon^2\eta_2(x) + O(\epsilon^3), & S &= S_o + \epsilon S_1 + \epsilon^2 S_2 + O(\epsilon^3). \end{aligned}\right\} \tag{3.2}$$

When we calculate the $O(\epsilon^0)$ solution, we recover the streamflow $\psi_o = y/h$, $\eta_o = h$, $R_o = R_h$ and $S_o = S_h$. At first order, we have

$$\psi_1(x,y) = -\frac{1}{h}\frac{\sinh(\pi y/L)}{\sinh(\pi h/L)}\cos\frac{\pi x}{L}, \qquad \eta_1(x) = \cos\frac{\pi x}{L}. \tag{3.3}$$

In order that R_1 is independent of x, we have to impose the condition

$$\tanh\frac{\pi h}{L} = \frac{\pi}{Lh^2}, \tag{3.4}$$

which relates the possible period $2L$ to the stream depth h. Equation (3.4) is familiar as the dispersion relation arising in linearized water-wave theory for small-amplitude waves (see, for example, Bland 1988). We can only solve (3.4) if $h > 1$, that is, bifurcation of waves only occurs from the subcritical stream. It follows (after a similar calculation for S_1) that both first-order corrections R_1 and S_1 vanish. With hindsight, this comes as no surprise. The symmetries of the boundary conditions force this 'pitchfork' bifurcation so that odd-order corrections make no contribution to either parameter.

If the required first-order terms are substituted into the second-order problem, we may solve to find that the second-order approximations to ψ and η are

$$\psi_2(x,y) = \frac{3h}{4}\left(1 - \frac{h^4L^2}{\pi^2}\right)\sinh\frac{2\pi y}{L}\operatorname{cosech}\frac{2\pi h}{L}\cos\frac{2\pi x}{L} + \frac{y}{2}, \tag{3.5}$$

$$\eta_2(x) = \frac{h^2}{4}\left(\frac{3L^2h^4}{\pi^2} - 1\right)\cos\frac{2\pi x}{L}. \tag{3.6}$$

After some algebra, it follows that the $O(\epsilon^2)$ expression for $R_{\text{wave}} \equiv R_w$ is

$$R_w = R_h + \left\{\frac{1}{2h} + \frac{h^2}{4}\left(1 - \tanh^2\frac{\pi h}{L}\right)\right\}\epsilon^2 > R_h + \left\{\frac{1}{2h}\right\}\epsilon^2. \tag{3.7}$$

We conclude that $R_w > R_h$. However, note that the bound is tight in the limit $L \to 0$, which is equivalent to the deep-water limit in h. We now wish to estimate S_w to second order. Using definition (2.8) of S, one can proceed by substitution of (3.2), (3.7) to find that, using (3.4),

$$S_w = S_h + \left\{\frac{1}{4} + \frac{h^3}{2}\left(1 - \tanh^2\frac{\pi h}{L}\right)\right\}\epsilon^2 > S_h + \tfrac{1}{4}\epsilon^2. \tag{3.8}$$

Therefore S_w is bounded above S_h. Whilst both flowforce and pressure head increase

for the wave relative to the streamflow, it is still not settled whether the bifurcating branch remains in the streamflow 'wedge' or whether it escapes.

To determine which case occurs, we compare the slopes of the streamflow and wave branch curves with respect to their parameterizations in the (R, S)-diagram at the point (R_h, S_h) where these intersect. We deduce that

$$\frac{(\mathrm{d}R/\mathrm{d}S)_h}{(\mathrm{d}R/\mathrm{d}S)_w} = \frac{1 + 2h^3(1 - \tanh^2(\pi h/L))}{2 + h^3(1 - \tanh^2(\pi h/L))}. \tag{3.9}$$

One can show using elementary calculus and (3.4) that this fraction is less than unity for h in the range $(1, \infty) \equiv (h^*, \infty)$. We conclude that the bifurcating branch always points into the streamflow wedge. These results are illustrated by some simple asymptotics. If the streamflow depth is close to the critical depth $h_* = 1$ then we put $h = 1 + \mu$, $\mu \ll 1$. Then we have

$$\left(\frac{\mathrm{d}R}{\mathrm{d}S}\right)_w \sim 1 + O(\mu^2), \qquad \left(\frac{\mathrm{d}R}{\mathrm{d}S}\right)_h \sim 1 - \mu + O(\mu^2). \tag{3.10}$$

At the other end of the streamflow branch, we set the small parameter μ to be $1/h$ to deduce that

$$\left(\frac{\mathrm{d}R}{\mathrm{d}S}\right)_w \sim 2\mu + O(\mu^2), \qquad \left(\frac{\mathrm{d}R}{\mathrm{d}S}\right)_h \sim \mu. \tag{3.11}$$

The 'deep-water' approximation (3.11) to $(\mathrm{d}R/\mathrm{d}S)_w$ is tight in practice before $h = 1.6$. The second-order approximations indicate that the predicted angle of incursion into the wedge has a maximum at approximately $h = 1.4$ and diminishes both for long wavelengths, and (especially) for deep water. Of course, to predict the size and direction of any possible turnaround in the wave branch, we need to calculate to (at least) the fourth order within this streamfunction formulation. The algebra involved is cumbersome and as we see in § 5, the effects seem rather subtle and involved. Instead, we concentrate on numerical solutions to gain more information about where the waves live in parameter space and the shape of the branches.

Before we move on, however, we return to the issue of the parameterization by ϵ. To leading order, ϵ is the wave amplitude. If one wishes to calculate only to second order, as we have done, an alternative approach would be to define ϵ by

$$R_2\epsilon^2 := R - R_h, \tag{3.12}$$

ensuring that $0 < \epsilon \ll 1$, and proceed in the obvious way to re-derive our results. Thus (3.7), (3.8) would imply that, to this order,

$$S_w = S_h + h\frac{1 + 2h^3(1 - \tanh^2(\pi h/L))}{2 + h^3(1 - \tanh^2(\pi h/L))}(R_w - R_h). \tag{3.13}$$

What we are doing here is, effectively, a series inversion. In fact, ϵ could be removed iteratively at each even order of calculation by repeated series inversion in order to express ϵ in terms of wave quantities, or equivalently yield $R = R(S)$. This is the kind of procedure carried out numerically in Fenton (1979) for cnoidal waves, because his primary concern was the provision of practical numerical values rather than an investigation of a particular parameter space.

4. The method of Teles da Silva & Peregrine

To complete our analysis of (R, S) parameter space, we now present a range of large-amplitude solution branches (with different periods), traced out in parameter space as the waveheight increases towards the extreme wave. The points in (R, S)-space were generated using a boundary-integral solver for the steady wave problem employed by Teles da Silva & Peregrine (1988). The numerical method of this scheme is based upon the work of Tanaka (1985, 1986) and Dold & Peregrine (1986). The wave problem is reduced to solving a nonlinear integro-differential equation posed on the upper boundary. Full details are given in the original paper.

Before we proceed, we need to summarize the alternative physical setup used within the program. A reference frame is chosen in which the wave is at rest with $y = 0$ as an undisturbed stream depth and $y = -h$ as the plane rigid bed. The water velocity $\boldsymbol{u}$ is given by

$$\boldsymbol{u} = (\Phi_x - c, \Phi_y), \tag{4.1}$$

where Φ is a velocity potential for the irrotational perturbation to a purely horizontal flow, and c, the wave velocity relative to the 'original' water velocity at the surface. That is, the perturbation velocity due to the wave at any point below a wave trough is chosen to be such that its phase average is zero and thus Φ is periodic. Now Φ satisfies Laplace's equation (1.1) but the boundary condition on the bed $y = -h$ is different in detail:

$$\Phi_y = 0. \tag{4.2}$$

Bernoulli's theorem and the free surface constant-pressure condition is written as

$$\tfrac{1}{2}(\Phi_x - c)^2 + \tfrac{1}{2}\Phi_y^2 + g\eta = B. \tag{4.3}$$

In solving the equations numerically, Teles da Silva & Peregrine (1988) take the wavenumber $k = 1$ and gravity $g = 1$ so that the wavelength is 2π. Once convergence to a wave profile η has been attained, the program outputs c and B but, in particular, also evaluates the integral quantities 'excess kinetic energy', and 'excess potential energy' as given by

$$2T = \int_0^{2\pi} \int_{-h}^{\eta} [\Phi_x^2 + \Phi_y^2]\, \mathrm{d}y\, \mathrm{d}x, \qquad 2V = \int_0^{2\pi} g\eta^2 \mathrm{d}x = \int_0^{2\pi} \int_0^{\eta} 2gy\, \mathrm{d}y\, \mathrm{d}x. \tag{4.4}$$

We now describe how the output is translated into results in the (R, S)-plane. First, the relative scalings between the two non-dimensionalizations are determined. To transfer from the dimensional water wave model (o-subscripts) to the Teles da Silva & Peregrine setup (p-subscripts) requires the scalings

$$x_o = \frac{L}{\pi} x_p, \quad y_o = \frac{L}{\pi} y_p, \quad \psi_o = \left(\frac{L^3 g}{\pi^3}\right)^{1/2} \psi_p, \quad R_o = \left(\frac{Lg}{\pi}\right) R_p, \quad S_o = \left(\frac{L^2 g}{\pi^2}\right) S_p. \tag{4.5}$$

For our model (D subscripts), recall the scales of §2:

$$x_o = \left(\frac{Q_o^2}{g}\right)^{1/3} x_D, \quad y_o = \left(\frac{Q_o^2}{g}\right)^{1/3} y_D, \quad R_o = (Q_o g)^{2/3} R_D, \quad S_o = Q_o^{4/3} g^{1/3} S_D. \tag{4.6}$$

Now observe that flux scales as the streamfunction, and hence $Q_o = (L^3 g/\pi^3)^{1/2} Q_p$. Thus we may eliminate Q_o upon equating expressions for variables in the dimensional formulation. Not forgetting translations, we obtain

$$x_D = Q_p^{-2/3} x_p, \quad y_D = Q_p^{-2/3} y_p, \quad R_D = Q_p^{-2/3} R_p, \quad S_D = Q_p^{-4/3} S_p. \tag{4.7}$$

Suppose the program is executed in a regime away from extreme waves. In this case, three parameters are used: vorticity (which is zero in our case), wave height H, and mean water depth, h_p. Typically, one follows a wave from close to its onset up towards an extreme waveform. As H is increased, c (and an internal parameter) are adjusted by the program in order that the mean water disturbance remains constant at its input value. Flat flows cannot be calculated since the Jacobian of the Newton solver for the discretized equations is then singular. Hence there is a difficulty in approaching the bifurcation point. Instead, bifurcation values of R and S are obtained from the usual dispersion relation. In order to plot (S, R) pairs in our non-dimensionalization, it remains to relate those integral quantities directly evaluated by the program to those we wish to evaluate, namely R and S. The flux $Q = Q_p$ is defined by

$$(-Q) := \int_{-h}^{\eta} (\phi_x - c)\mathrm{d}y. \tag{4.8}$$

Integration between 0 and 2π yields

$$Q_p = ch - \frac{T}{\pi c}. \tag{4.9}$$

For pressure head, we just apply the scaling (4.7) to

$$R_p = B + h. \tag{4.10}$$

The flowforce calculation is more involved (see Doole 1994). The definition of flowforce becomes, using (2.8)

$$S_p = \int_{-h}^{\eta} (p + (\Phi_x - c)^2)\mathrm{d}y. \tag{4.11}$$

Integrating from 0 to 2π, we obtain after some manipulation

$$S_p = 2Bh - \frac{3}{2\pi}V + \frac{1}{2}gh^2. \tag{4.12}$$

5. Numerical results for the irrotational (R, S)-diagram

The procedure to obtain numerical (R, S) bifurcation diagrams is as follows. The program is run with input values in the p-non-dimensionalization as this is more convenient for investigative purposes. An initial depth h_p is chosen along with a small wave height H, usually around 10^{-2}. We continue in the wave height parameter (directly or indirectly) towards the Stokes' corner wave, with the corresponding values of R_p and S_p being rescaled using Q_p to give the output in our non-dimensionalization. Computations for this paper used generally 100 points per wave, with around 60 (S, R) points per wave branch. A full discussion of accuracy and error control is given in Doole (1994). Experimentation showed that the wave branches emanating from the depths shown in table 1 exhibit the full range of possible behaviours. In the table, we record the stream depth with respect to both non-dimensionalizations, the period of the bifurcating wave (which shows the variation expected from (3.4)), the (S, R) bifurcation points and the height of the extreme wave. (In the non-dimensionalization of Teles da Silva & Peregrine 1988, the extreme wave height *increases* with h_p.)

There are many qualitative features which vary as the streamflow depth is increased by, say, 25% from its critical value. We begin close to the cusp with $h_p = 1.1$, 1.2 and 1.3. In figure 4, we show the corresponding (R, S)-diagram. The branch leaves

h_p	Stream, h_D	Period, $2L$	Bifurcation S_b	Bifurcation R_b	Extreme height
1.1	1.11175893	6.35035216	1.5175	1.5162	0.6452
1.2	1.12909815	5.91194411	1.5231	1.5212	0.6315
1.21	1.13085976	5.87223256	1.5237	1.5218	0.6300
1.3	1.14689906	5.54321484	1.5296	1.5270	0.6169
1.4	1.16503081	5.22864606	1.5370	1.5334	0.6018
1.45	1.17418437	5.08801239	1.5410	1.5368	0.5944
1.48	1.17969698	5.00828023	1.5435	1.5390	0.5898
1.5	1.18337897	4.95692623	1.5452	1.5404	0.5865
1.505	1.18430022	4.94430416	1.5457	1.5408	0.5859
1.51	1.18522176	4.93176683	1.5461	1.5412	0.5852
1.52	1.18706562	4.90694292	1.5470	1.5419	0.5837
1.53	1.18891047	4.88244756	1.5479	1.5426	0.5822
1.54	1.19075621	4.85827397	1.5488	1.5434	0.5806
1.55	1.19260277	4.83441560	1.5497	1.5441	0.5791
1.6	1.20184484	4.71963365	1.5543	1.5480	0.5714
1.8	1.23880752	4.32425400	1.5745	1.5646	0.5415
2.0	1.27540127	4.00679126	1.5974	1.5828	0.5309
2.05	1.28444884	3.93679392	1.6034	1.5875	0.5064
2.1	1.29344635	3.86998244	1.6096	1.5923	0.4998
2.5	1.36331915	3.42639473	1.6628	1.6323	0.4515
3.0	1.44463487	3.02563618	1.7357	1.6842	0.4027

TABLE 1. Parameter values for wave branches in the (R, S)-diagram.

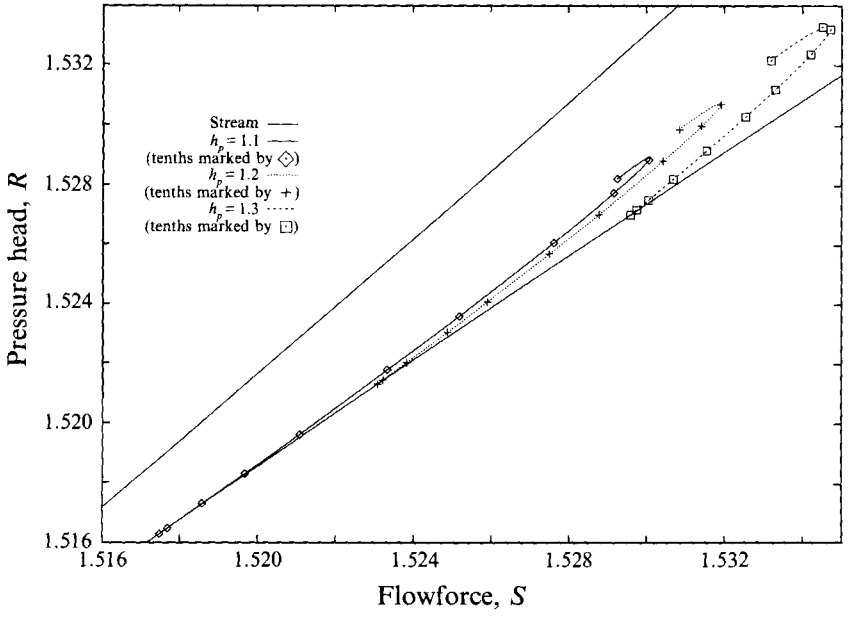

FIGURE 4. The (R, S)-diagram for irrotational flow with $h_p = 1.1$, 1.2 and 1.3. Tenths of extreme wave height as marked.

the streamflow locus with the onset of (sinusoidal) waves and wave height increases along the branch until the extreme wave is reached. The marked points correspond to 10% increments of extreme wave height. The first two branches are fairly evenly parameterized by wave height, whilst in this respect the $h_p = 1.3$ branch appears more 'transitional' (see later). Observe that the $h_p = 1.1$ branch, for much of its length, is almost parallel to the wedge (in line with the long-wave theory of Doole 1994). Moreover, the subsequent branches lift up away from the streamflow in line with § 3.

Considering figure 4 as a bifurcation diagram, it may seem strange that the bifurcating curves just 'stop', in apparent contradiction of Rabinowitz's Global Bifurcation Theorem. However, the problem is not a 'loss of compactness', but rather that R and S are first-derivative 'measures' (norms) of the wave. It is the second derivative of the wave profile that experiences a singularity at the Stokes' corner wave and hence there is no discrepancy.

If we now focus on $h_p = 1.3$ (figure 5), we observe two kinds of fold. The first is that associated with the maximum value of S (greater than the bifurcation value S_b). The second fold at the end of the wave branch is a feature common to all branches, but we describe its cause now. Until the decade 1972–1982, many benevolent properties were assumed for water waves, for instance uniqueness of periodic waves. It was only as steep waves were calculated much more accurately that unexpected phenomena were revealed. Prime amongst these was the discovery that the maxima of 'important integral properties' do not occur at the extreme wave. The highest value of such quantities actually occurs at around 85% of the extreme wave height. Moreover, the wave properties then go through a decaying oscillation as the extreme wave limit is approached. However, these oscillations decay so fast as a function of wave height that it seems beyond double precision computations to resolve more than three of them. (An exception is the recent, precise work of Chandler & Graham 1993.) Two points are worth noting. By plotting R against S, the uneven parameterization of the curves by H, as well as the required scale, obscures the number of oscillations actually present in the data. In addition, the plotting of several oscillations, though achievable with the code (Teles da Silva & Peregrine 1988; Doole 1994), is not the main thrust of the work. The global branch behaviour is of much greater importance.

The phenomenon of premature maxima was discovered by Schwartz (1974) and Longuet-Higgins (1975) and accurately numerically plotted by continuation in Chen & Saffman (1980). The phenomena very close to the extreme wave were first described (with matched asymptotics) by Longuet-Higgins & Fox (1978). The maximum point has been associated with mechanisms for instability, bifurcation and wave breaking (reviewed by Jillians 1989, for example). In the above references, the main emphasis is on c, T/V and so on. However, the same behaviour is exhibited by R and S. Consequently, when plotted against each other, a 'spiral' results. However, the continuation of the spiral beyond our current ability to resolve it, will depend on whether the oscillations of R and S remain out of phase. These remarks raise the possibility of another kind of non-uniqueness in the (R, S)-diagram. At high wave steepness, successive secondary subharmonic bifurcations occur (as discovered by Chen & Saffman 1980; and organized since into a theory by Aston 1991 and Baesens & Mackay 1992). These give rise to branches terminating at lower wave heights but with similar oscillatory behaviour in integral properties. In (R, S)-space, this could lead to the intersection of individual spirals and hence multimode interactions close to the extreme wave. However, symmetric bifurcation theory may be able to exclude this (cf. Aston's 1991 analysis of the conjectures of Jones & Toland 1985, 1986).

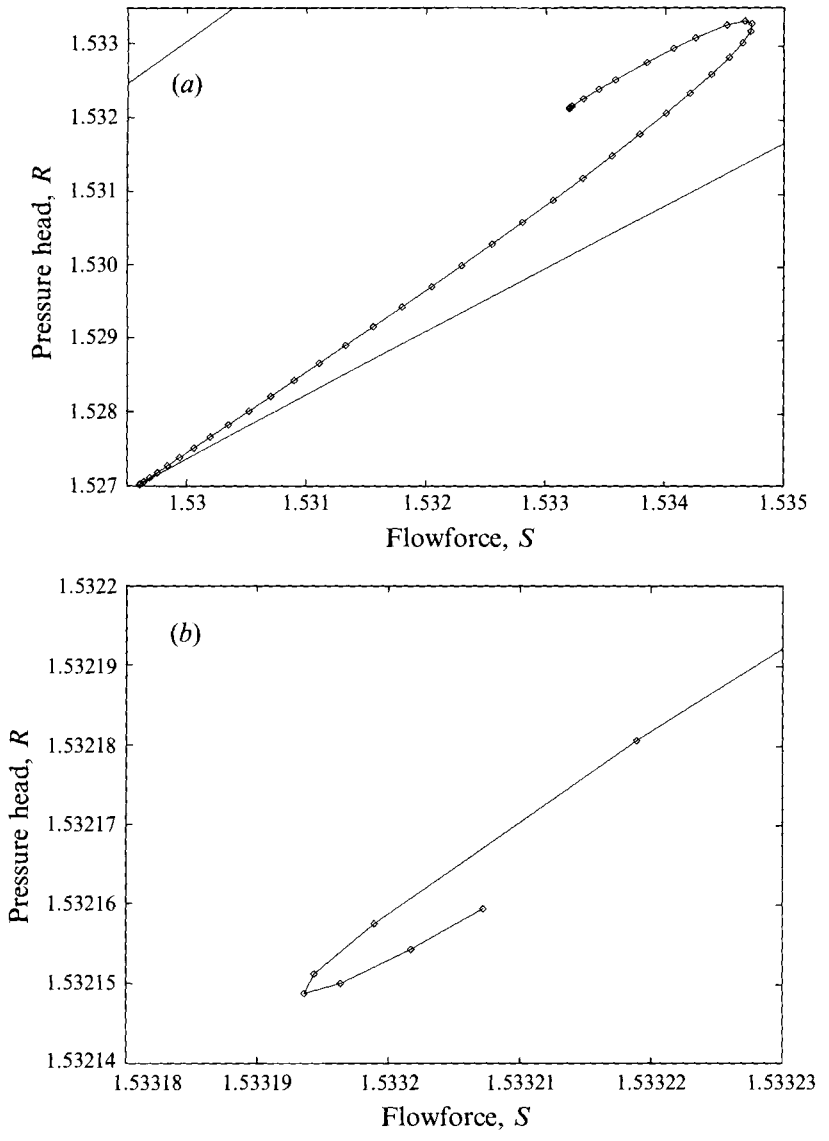

FIGURE 5. Focus on the $h_p = 1.3$ wave branch in the (R, S)-diagram. (*a*) Computed points shown. (*b*) Close-up of the terminal branch fold.

In figure 6, we see that the other extreme ($h_p = 1.8$, 2.0 and 2.5) is quite different: the branches 'point' in the opposite direction. The labels indicate 'tenths' of extreme wave height as before. At the resolution of figure 6, it appears that the branches do not initially increase their R and S values. In fact, the curves of figure 6 have flipped over the vertical very rapidly and the effect of the exponential deep-water limit is to compress this fold onto the streamflow cusp. Resolution of the flip-over needs wave heights of the order of 10^{-5} for which the variation in R and S cannot be computed in a sufficiently robust and reliable manner. We will see how the fold shrinks down to the streamflow locus in other figures. Of course, such a feature is only of theoretical interest, since for such wave heights, any practical theory should include surface tension effects and/or viscous dissipation.

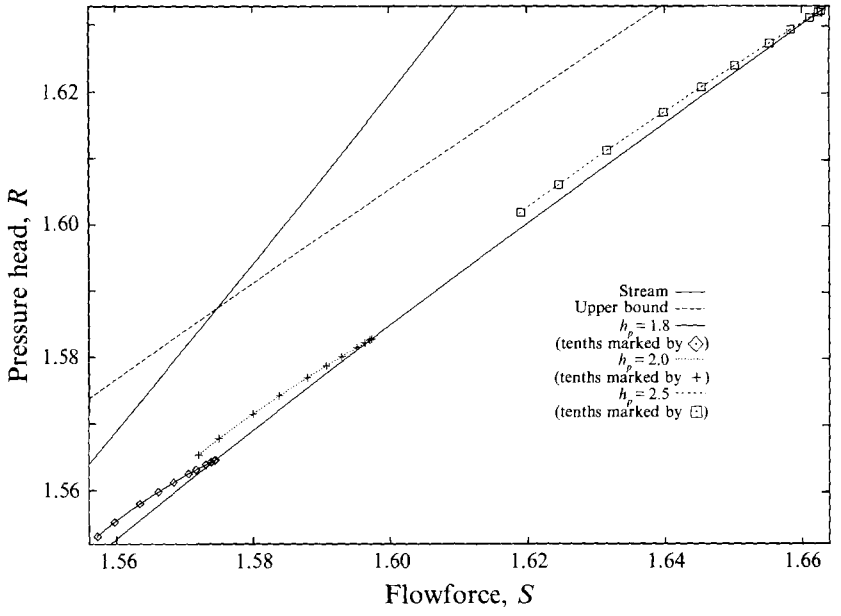

FIGURE 6. The (R, S)-diagram for irrotational flow with $h_p = 1.8$, 2.0 and 2.5. Tenths of extreme wave height as marked.

Therefore, between $h_p = 1.3$ and $h_p = 1.8$, a dramatic transition must take place. Visually, the main changes occur between $h_p = 1.45$ and $h_p = 1.55$ (figures 7 and 8). The branch buckles over prior to stretching out again for deep water. It appears that it is the part of the branch corresponding to small wave heights that is 'compressed', since the parameterization indicated by the 10% markers is now most uneven. However, once $h_p = 1.6$, branch shape differs little from those of figure 6. Note that at approximately the same depth, the nature of the graphs of the second-order corrections changes significantly.

In figures 7 and 8, we see that the loci do not sit inside each other in a simple way. Branches corresponding to different periods can cross and thus a new type of non-uniqueness appears. In this transition zone, the intersections can occur some distance up the branch. In figure 9, we look at how this changes in the two extremes of the long-wave and deep-water regimes. In both, the crossings tend to be closer to the terminal (R, S)-values. The branch length compression during the transition of behaviour can be clearly seen in the summary, figure 3. In the same figure, we have plotted the analytical bounds of Keady & Norbury (1975, 1978) for a periodic wavetrain. From the diagram, we can see that the bounds are not tight. However, the influence of the upper bound is apparent. Long-wave theory (Doole 1994) indicates that wave branches like that emanating with $h_p = 1.1$ cannot fold inside the region where the theory remains applicable, hence the shape and direction of such branches. However, as we move away from the cusp, the influence of the upper bound becomes dominant and forces wave branches to turn. In passing, we note that the fact that all the branches fold undermines a remark of BL. Waves lie on *both sides* of the curve corresponding to the waves of greatest height. Keady & Norbury (1978) reported a personal communication of E. D. Cokelet in 1976 stating that his steep wave solutions (Cokelet 1977) also had this property. However, the upper bound of Keady & Norbury in figure 3 has the properties of Benjamin & Lighthill's 'third

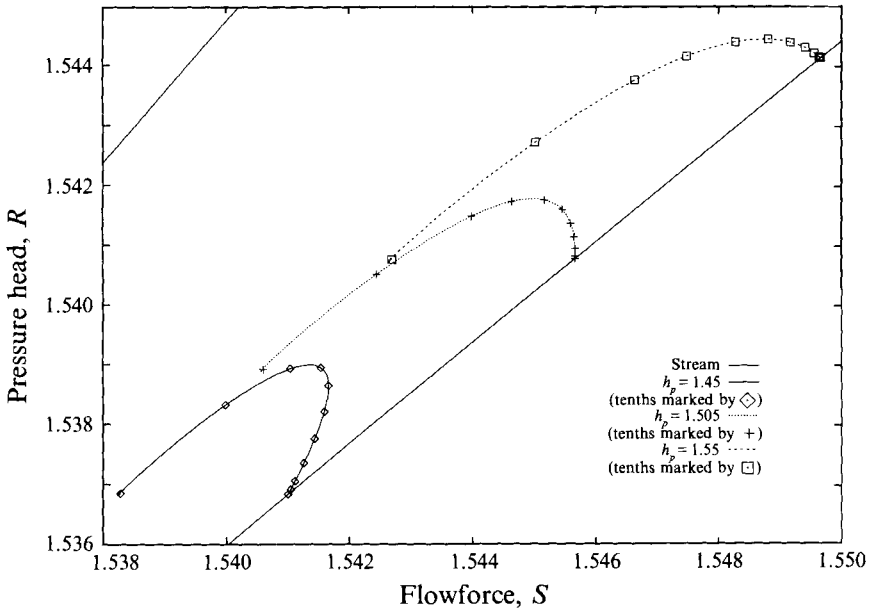

FIGURE 7. The (R, S)-diagram for $h_p = 1.45$, 1.505 and 1.55 in the transitional region. Tenths of extreme wave height as marked.

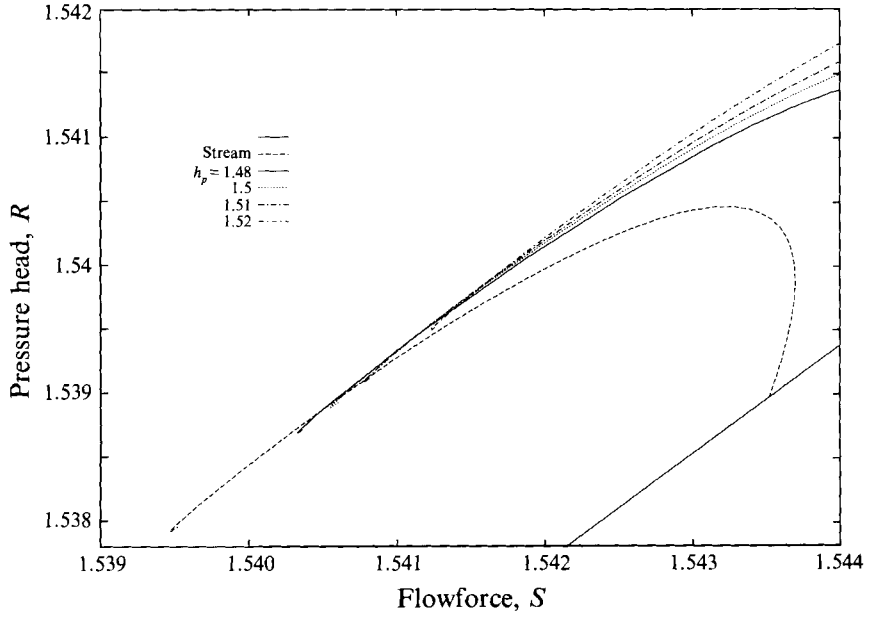

FIGURE 8. Intersection of wave branches in the transitional region of the irrotational (R, S)-diagram.

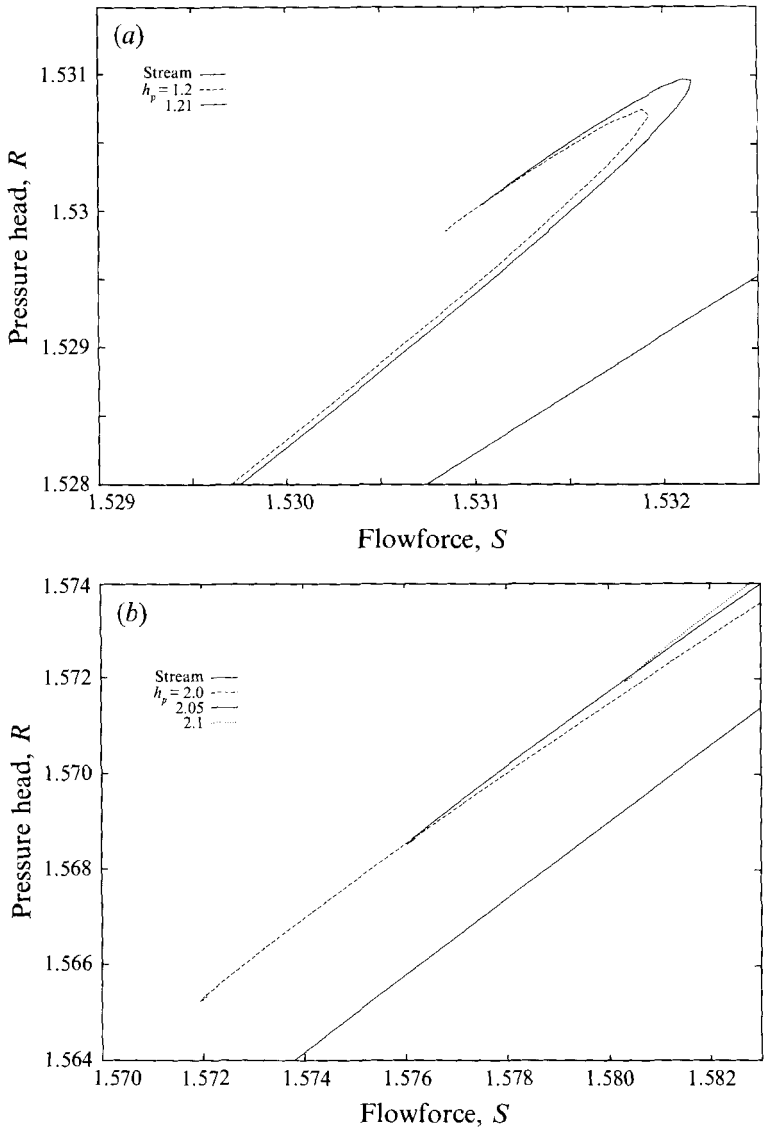

FIGURE 9. Intersection of wave branches (*a*) closer to the cusp and (*b*) in the 'deep-water' region.

line completing the (R, S)-diagram'. The reason for Benjamin & Lighthill's error was probably the (then-unsuspected) existence of 'premature' maxima in the integral properties of water waves.

Two other features are clear from figure 3. First, that the large-amplitude branches remain remarkably close to the subcritical stream branch and secondly, that it is only the cnoidal-wave region that is more densely 'filled' with wave branch loci. We make two final remarks. First, the effects at second order upon R and S in the presence of constant vorticity may be indicators as to the likely influence of higher-order terms on irrotational flow. In Doole (1994), it is shown that the introduction of a little vorticity can give strong corrections to the wave branch slope, causing rotation of the branch, especially away from the long-wave region. Secondly, the distinct branch behaviour in the long-wave limit may be related to stability properties

for channel flows under a sluice as considered in Benjamin (1956) and Budden & Norbury (1977, 1984). Experiments indicate that if the Froude number F of the incident subcritical flow is greater than about 0.8, waves always appear downstream, despite all attempts to avoid them. Theoretically, it appears that as $F \to 1-$, undulation is the preferred downstream profile (Budden & Norbury 1984). This exchange of stability between streamflow and wave corresponds to a subcritical depth, in our non-dimensionalization, of around 1.13. That this is close to the value of h_D at which the wave branch stops taking a pure long-wave form may be just numerical coincidence. However, one should not lightly dismiss features of the (R, S)-diagram because of its role in highlighting wave transitions and changes in wave energetics. This is even more the case for the 'S-increase' fold which is visually lost when $h_p \sim 1.505$. Turning points in bifurcation diagrams are often associated with changes in stability. The physical repercussions of this fold are not clear, not least because it is hard to judge when the feature becomes smaller than lengthscales for which the model $[P_\eta]$ has physical relevance.

6. Conclusions

We have presented numerical computations of the (global) wave branches (each characterized by a non-dimensionalized wavelength $L \in (0, \infty)$) in the energy/momentum flux (R, S)-diagram normalized for mass flux $Q = 1$. The exact equations of the steady ideal water wave problem $[P_\eta]$ were solved by a boundary-integral method after translation into our non-dimensionalization. The numerical (R, S)-diagram is consistent with the local mathematical arguments of § 3, most accurately nearer the cusp at h_*, the critical flow depth. In the figures of § 5, we saw the overlapping of different constant-period branches so that a single (Q, R, S) triple may correspond to more than one wave. This raises the possibility of a modulational instability of water waves based on (R, S) energetics, but any mechanism remains unclear. Of course, the intersections occur in a *projected* plane and the 'continuous' bifurcation of wave branches along the subcritical branch is unfolded with the introduction of an L-axis (cf. the discussion of § 2). This new type of 'non-uniqueness' is not associated with the (now well-understood) loss of uniqueness via secondary bifurcations near the premature maxima of wave properties with respect to wave height.

In our view, the most important feature of the (R, S)-diagram that we have uncovered is the closeness of all of the wave branches to the subcritical branch. In addition, the (R, S)-plane may well be a 'natural' bifurcation diagram but the transitions of interest, from 'long-waves' to 'deep-water' are highly compressed geometrically. Of course, this may reflect our particular non-dimensionalized value of flux, and thus the kind of 'slice' we are taking through multi-dimensional physical parameter space. Higher-order series may improve our understanding of the detail of the figures of § 5, but it seems more likely that a competing small parameter or a rescaling is required to unfold the normal form. However, as figure 3 shows, as S increases from 1.54 to 1.55, the maximum-S fold point on a branch of waves of given wavelength rapidly moves from large-amplitude to very small-amplitude waves. Hence, transitions at constant energy R that decrease S (for instance, obstructions in the flow that absorb momentum) have complicated, but limited possibilities, and further work on stability is needed to resolve this.

The investigations of § 5 could be extended in a number of ways. For instance, the known subharmonic secondary bifurcation of waves has yet to be plotted in the

(R, S)-diagram. For irrotational flow, this immediately suggests possible interactions between waves of distinct periods as loci spiral in parameter space. It is also of physical interest that other loci, such as lines of constant wave steepness are plotted in the (R, S)-plane. The (R, S)-diagram should also be plotted for non-zero constant vorticities. In this case, the global behaviour is completely open; the basic local bifurcation theory is more complicated (Doole 1994), and the bounds of Keady & Norbury (1978) are weaker. To aid such computations, one step would be to improve those bounds. Very recently, Benjamin (1995) has extended the methods of Keady & Norbury (1978) to improve the lower bound in the irrotational case so that it coincides with the streamflow (for monotone Stokes' waves). The results of § 5 show that refinement of the upper bound is also needed. Of course, this is more difficult since R and S are singular in the 'deep-water' limit.

The authors thank Howell Peregrine for permission to use the program `stchy.f` with which the computations of this paper and others in Doole (1994) were carried out. The authors are also grateful to Brooke Benjamin for the interest he has shown in this work, and to Chris Budd and Howell Peregrine for informative discussions. S.D. acknowledges funding from the EPSRC UK (as the SERC) via a Research Studentship, and from Corpus Christi College, Oxford whilst Garside Senior Scholar.

REFERENCES

Aston, P. J. 1991 Analysis and computation of symmetry-breaking bifurcation and scaling laws using group theoretic methods. *SIAM J. Math. Anal.* **22**, 181–212.

Baesens, C. & Mackay, R. S. 1992 Uniformly travelling waves from a dynamical systems viewpoint: ome insights into bifurcations from Stokes' family. *J. Fluid Mech.* **241**, 333–347.

Benjamin, T. B. 1956 On the flow in channels when rigid obstacles are placed in the stream. *J. Fluid Mech.* **1**, 227–248.

Benjamin, T. B. 1984 Impulse, flow force and variational principles. *IMA J. Appl. Maths* **32**, 3–68.

Benjamin, T. B. 1995 Verification of the Benjamin-Lighthill conjecture about steady water waves. *J. Fluid Mech.* **295**, 337–356.

Benjamin, T. B. & Lighthill, M. J. 1954 On cnoidal waves and bores. *Proc. R. Soc. Lond.* A **224**, 448–460 (referred to herein as BL).

Benjamin, T. B. & Olver, P. J. 1982 Hamiltonian structure, symmetries and conservation laws for water waves. *J. Fluid Mech.* **125**, 137–185.

Bland, D. R. 1988 *Wave Theory and Applications.* Oxford University Press.

Bridges, T. J. 1992 Spatial Hamiltonian structure, energy flux and the water-wave problem. *Proc. R. Soc. Lond.* A **439**, 297–315.

Budden, P. & Norbury, J. 1977 Sluice gate problems with gravity. *Math. Proc. Camb. Phil. Soc.* **81**, 157–175.

Budden, P. & Norbury, J. 1984 Stability of a subcritical flow under a sluice gate. *Q. J. Mech. Appl. Maths* **37**, 293–310.

Chandler, G. A. & Graham, I. G. 1993 The computation of water waves modelled by Nekrasov's equation. *SIAM J. Numer. Anal.* **30**, 1041–1065.

Chappelear, J. E. 1961 Direct numerical calculation of wave properties. *J. Geophys. Res.* **66**, 501–508.

Chen, B. & Saffman, P. G. 1980 Numerical evidence for the existence of new types of gravity-waves of permanent form on deep-water. *Stud. Appl. Maths* **62**, 1–21.

Cokelet, E. D. 1977 Steep gravity waves in water of arbitrary uniform depth. *Phil. Trans. R. Soc.* A **286**, 183–220.

De, S. C. 1955 Contributions to the theory of Stokes waves. *Proc. Camb. Phil. Soc.* **51**, 713–736.

Dixon, A. 1989 Momentum disturbances and wave trains. *J. Fluid Mech.* **207**, 295–310.

DOLD, J. W. & PEREGRINE, D. H. 1986 An efficient boundary-integral method for steep unsteady water waves. In *Numerical Methods for Fluid Dynamics II* (ed. K. W. Morton & M. J. Baines), pp. 671–679. Oxford University Press.

DOOLE, S. H. 1994 Steady gravity waves on flows with vorticity: bifurcation theory and variational principles. DPhil thesis, Oxford University, UK.

FENTON, J. D. 1979 A high-order cnoidal wave theory. *J. Fluid Mech.* **94**, 129–161.

FENTON, J. D. 1985 A fifth order Stokes theory for steady waves. *J. Waterway, Port, Coastal, Ocean Engng Div. ASCE* **111**, 216–234.

JILLIANS, W. J. 1989 The superharmonic instability of Stokes' waves in deep water. *J. Fluid Mech.* **204**, 563–579.

JONES, M. C. W. & TOLAND, J. F. 1985 The bifurcation and secondary bifurcation of capillary–gravity waves. *Proc. R. Soc. Lond.* A **399**, 391–417.

JONES, M. C. W. & TOLAND, J. F. 1986 Symmetry and the bifurcation of capillary–gravity waves. *Arch. Rat. Mech. Anal.* **96**, 29–53.

KEADY, G. & NORBURY, J. 1975 Water waves and conjugate streams. *J. Fluid Mech.* **70**, 663–671.

KEADY, G. & NORBURY, J. 1978 Waves and conjugate streams with vorticity. *Mathematika* **25**, 129–150.

KELVIN, LORD 1886 On stationary waves in flowing water II. *Phil. Mag.* **5**, 445–452.

LONGUET-HIGGINS, M. S. 1975 Integral properties of periodic gravity waves of finite amplitude. *Proc. R. Soc. Lond.* A **342**, 157–174.

LONGUET-HIGGINS, M. S. & FOX, M. J. H. 1978 Theory of the almost largest wave. Part 2. Matching and analytic extension. *J. Fluid Mech.* **85**, 769–786.

MIELKE, A. 1991 *Hamiltonian and Lagrangian Flow on Center Manifolds with Applications to Elliptic Variational Problems.* Lecture Notes in Mathematics, Vol. 1489. Springer.

OLVER, P. J. 1982 A nonlinear Hamiltonian structure for the Euler equations. *J. Math. Anal. Appl.* **89**, 233–250.

RADDER, A. C. 1992 An explicit Hamiltonian formulation of surface waves in water of finite depth. *J. Fluid Mech.* **237**, 435–455.

SCHWARTZ, L. W. 1974 Computer extension and analytic continuation of Stokes' expansion for gravity waves. *J. Fluid Mech.* **62**, 553–578.

TANAKA, M. 1985 The stability of steady gravity waves. Part 2 *J. Fluid Mech.* **156**, 281–289.

TANAKA, M. 1986 The stability of solitary waves. *Phys. Fluids* **29**, 650–655.

TELES DA SILVA, A. F. T. & PEREGRINE, D. H. 1988 Steep, steady surface waves on water of finite depth with constant vorticity. *J. Fluid Mech.* **195**, 281–302.

URSELL, F. 1953 The long wave paradox in the theory of gravity waves. *Proc. Camb. Phil. Soc.* **49**, 685–694.

WILLIAMS, J. M. 1981 Limiting gravity waves in water of finite depth. *Phil. Trans. R. Soc. Lond.* A **302**, 139–188.